ROYAL SOCIETY OF CHEMISTRY

PAPER

Spectroscopic and nonlinear optical properties of the four positional isomers of 4α-(4-*tert*-butylphenoxy)phthalocyanine†

Grace N. Ngubeni,[a] Jonathan Britton,[a] John Mack,[a] Edward New,[b] Ian Hancox,[b] Marc Walker,[bc] Tebello Nyokong,[a] Tim S. Jones[b] and Samson Khene*[a]

The spectroscopic and nonlinear optical properties of the positional isomers of metal free 4α-(4-*tert*-butylphenoxy) phthalocyanine are presented. Second order nonlinear polarizability (β), imaginary hyperpolarizability (Im(γ)) and imaginary susceptibility (Im[$\chi^{(3)}$]) values were determined for the four positional isomers. The measured β values of the four isomers displayed the following trend, C_{4h} (34.0×10^{-5} m MW^{-1}) > D_{2h} (28.8×10^{-5} m MW^{-1}) > C_{2v} (22.8×10^{-5} m MW^{-1}) > C_s (13.7×10^{-5} m MW^{-1}).

1. Introduction

Organic materials with second-order nonlinear optical (NLO) material properties are useful in applications such as optical data processing and storage devices and can be easily processed and integrated into optical devices.[1,2] Phthalocyanines exhibit large and rapid nonlinearities to incident pulsed laser light, which can be fine-tuned by rational modification of the molecular structure.[3–5] Phthalocyanine molecules are known to have large third-order optical nonlinearities which arise from the highly delocalised two dimensional heteroaromatic 18-π electron system,[5–8] and hence have been intensively investigated for their NLO properties. In most studies, the NLO properties of tetra-substituted phthalocyanines have been studied as a mixture of possible positional isomers.[9] Since the substituents at either the non-peripheral and peripheral positions (referred to throughout as the α- and β-positions, respectively) of each fused benzene ring can be orientated in two directions with respect to the rest of the ligand, there is scope for four positional. The substitution patterns of these isomers are labeled as D_{2h}, C_{4h}, C_{2v} and C_s throughout to aid comparison with D_{4h} symmetry metalated complexes in the literature,[10] but it should be noted that the free base phthalocyanine in this study has lower symmetry than this due to the absence of a four-fold axis of symmetry. The separation of the four isomers by column chromatography is usually highly challenging, but bulky substituents can be introduced to facilitate their chromatographic separation.

In this study, the four positional tetra-α-substituted (4α) isomers of metal free 1, 8(or 11), 15(or 18), 22(or 25)-(4-*tert*-butylphenoxy)phthalocyanine have been fully separated and their NLO properties have been measured separately, to identify which isomer provides the largest contribution to the observed NLO response. Substitution at the non-peripheral α-positions is known to have a greater effect on the energies of the four frontier π-MOs of the phthalocyanine π-system.[10] It has been reported that the second order NLO factor has symmetry restrictions,[11] and is zero in centrosymmetric systems, whereas the third order NLO factor has no symmetry restrictions and can take place in any material possessing a highly polarizable delocalized π-system.[12] The optimization of the second order nonlinear absorption coefficient (β) has a direct impact on the macroscopic second order NLO response.[13] The Z-scan technique has been employed to determine the second and third order NLO properties of the four regioisomers, and their spectroscopic and photophysical properties have been determined using a range of different spectroscopic techniques, including magnetic circular dichroism (MCD), time correlated single photon counting spectroscopy (TCSPC), and UV-visible absorption spectroscopy. A combined analysis of the optical spectral data and the results of density functional theory (DFT) calculations are used to characterise the physical properties of the isomers.

2. Experimental

2.1 Material

4-*tert*-Butylphenol, column chromatography silica, pentanol, *N*,*N*-dimethylformamide (DMF) and lithium were purchased from Sigma Aldrich. Toluene was supplied by Beckman/B&M Scientific, while acetone, methanol, acetic acid, hexane acetonitrile

[a] *Department of Chemistry, Rhodes University, PO Box 94, Grahamstown 6140, South Africa. E-mail: s.khene@ru.ac.za*
[b] *Department of Chemistry, University of Warwick, Coventry CV4 7AL, UK*
[c] *Department of Physics, University of Warwick, Coventry, UK*
† Electronic supplementary information (ESI) available: Calculated electronic absorption spectra. See DOI: 10.1039/c5tc01601k

This journal is © The Royal Society of Chemistry 2015

J. Mater. Chem. C, 2015, **3**, 10705–10714 | **10705**

and chloroform were purchased from BDH laboratory reagents and Merck. 4α-(4-*tert*-butylphenoxy)phthalocyanine was synthesized with modifications according to the literature method.[14,15]

2.2 Instrumentation

Electronic absorption spectra were recorded on a Shimadzu UV-2550 spectrophotometer. Solid state UV-visible absorption spectra were measured using a Perkin Elmer LAMBDA 25 spectrometer. Isomer thin films were formed by spin coating from 1,2-dichlorobenzene onto quartz substrates. Magnetic circular dichroism (MCD) spectra were measured on a Chirascan Plus spectropolarimeter equipped with a permanent magnet, which produces a magnetic field of 1 T (1 tesla). A solid state large area avalanche photodiode (LAAPD) was used as the detector. Fluorescence lifetimes were measured with a FluoTime 300 EasyTau spectrometer (PicoQuant GmbH) using a time correlated single photon counting (TCSPC) technique. The samples were excited at 670 nm with a diode laser (LDH-P-670, 20 MHz repetition rate, 44 ps pulse width, Pico-Quant GmbH). The detector employed was a Peltier cooled photomultiplier (PMA-C 192-M, PicoQuant GmbH). Mass spectral data were collected on a Bruker AutoFLEX III smart-beam MALDI-TOF mass spectrometer using α-cyano-4-hydroxycinnamic acid as the matrix in positive ion mode.

All Z-scan experiments described in this study were performed using a frequency-doubled Nd:YAG laser (Quanta-Ray, 1.5 J/10 ns fwhm pulse duration) as the excitation source. The laser was operated in a near Gaussian transverse mode at 532 nm (second harmonic), with a pulse repetition rate of 10 Hz and an energy range of 0.1 µJ–0.1 mJ, which was monitored with an energy detector (Coherent J5-09). The low repetition rate of the laser prevents cumulative thermal non-linearities. The beam was spatially filtered to remove the higher order modes and tightly focused with a 15 cm focal length lens. No damage was detected between runs when the sample was moved or replaced. Ultra-violet photoemission spectroscopy (UPS) measurements were carried out in a Kratos Axis Ultra DLD system (Kratos Analytical, Manchester UK), with a base pressure in the analysis chamber of approximately 2×10^{-10} mbar. The sample was illuminated with He I (alpha) emission (21.2 eV) from a double differentially-pumped Kratos Vacuum Ultraviolet Source. Photoelectrons ejected from a 110 micrometer area of the sample were collected using the delay line detector at a pass energy of 5 eV and a step size of 0.01 eV.

The Gaussian 03 software package[16] running on an Intel/ Linux cluster was used to perform a series of B3LYP geometry optimizations with 6-31G(d) and SDD basis sets. Gaussview 4.1 was used for all visualizations of molecular orbitals (MOs) and properties.[16] The B3LYP exchange–correlation density functional employs Becke's method for using Lee–Yang Parr's gradient-correction, which includes a hybrid of semi-empirical Hartree–Fock and DFT exchange. B3LYP/6-31G(d) formalism was used to perform single-point energy calculations to determine the NLO response (β), following literature methods,[17] using $H_2(OH)_4Pc$ as a model compound. TD-DFT calculations for the four positional isomers of a $H_2(OH)_4Pc$ model compound were carried out using the B3LYP functional of the Gaussian 09 software package with 6-31G(d) basis sets.[18]

2.3 Synthesis, separation and characterisation of unmetalated 4α-(4-*tert*-butylphenoxy)phthalocyanine

4α-(4-*tert*-Butylphenoxy)phthalocyanine was readily identified as a free base phthalocyanine through optical spectroscopy.[10] The four possible positional isomers of 4α-(4-*tert*-butylphenoxy)-phthalocyanine with D_{2h}, C_{4h}, C_{2v} and C_s symmetry are shown in Fig. 1 and 2. The isomers were successfully separated by silica gel flash column chromatography. Fig. 3 shows the four fractions that were obtained in order of elution. Fraction A (blue) was eluted first followed by fractions B (light green), C (light green) and D (olive green) with minimal overlap between the fractions. DCM was used to elute fractions A, B and C, while a mixture of DCM and MeOH (10 : 1 ratio) was used to elute fraction D. The optical and IR spectral data and MALDI-MS measurements were consistent with what would be anticipated for one of the four isomers of 4α-(4-*tert*-butylphenoxy)phthalocyanine. ^{1}H NMR spectra were measured, but the isomers could not be definitively identified on this basis due to peak broadening issues that are often encountered with phthalocyanines.[19,20]

Fraction A (C_s symmetry isomer). IR [(KBr) ν_{max}/cm^{-1}]: 1246 (C–O–C); 1362 (CH$_3$); 1486, 1506, 1584 (C=C); 2853, 2922, 2954 (–C–H); 3060, 3289 (=C–H), UV/vis (DCM): λ_{max} nm (log ε): 714
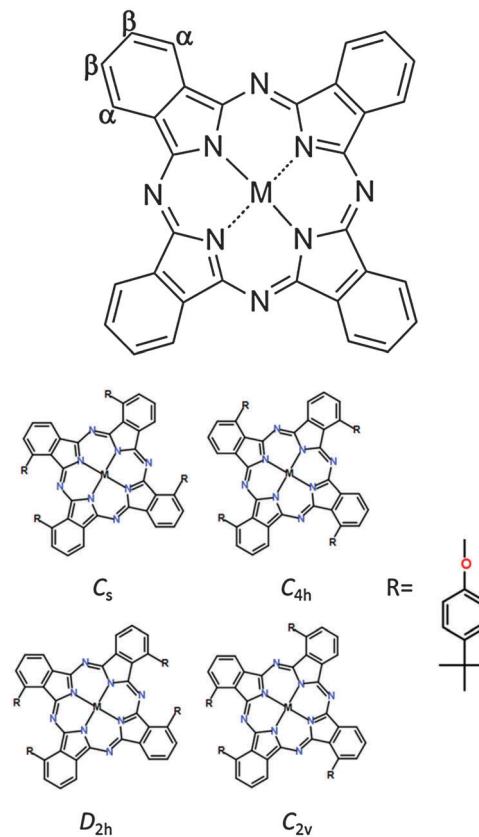

Fig. 1 The α- and β-positions of phthalocyanine (top). The four positional isomers of 1, 8(or 11), 15(or 18), 22(or 25)-tetrasubstituted phthalocyanines (bottom).
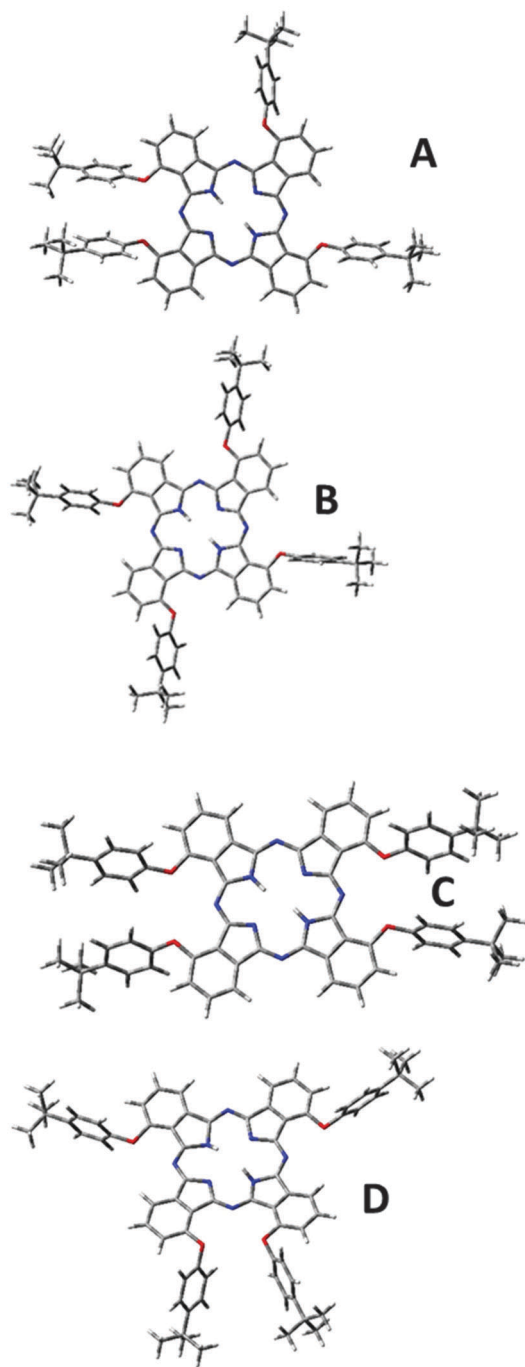
Fig. 2 Optimised structures of 4α-(4-*tert*-butylphenoxy)phthalocyanine positional isomers with C_s (A), C_{4h} (B), D_{2h} (C), and C_{2v} (D) symmetry substitution patterns. The structures were optimised at the B3LYP level of theory with SDD basis set.

(5.15), 683 (5.07), 654 (4.64), 620 (4.47), 357 (4.73), 333 (4.77). MS (MALDI-TOF) *m/z*: calcd 1107.0; found 1107.7 [M − H]⁺.

Fraction B (C_{4h} symmetry isomer). IR [(KBr) ν_{max}/cm^{-1}]: 1246 (C–O–C); 1362 (CH$_3$); 1486, 1506, 1583 (C=C); 2865, 2955 (–C–H); 3036, 3290 (=C–H), UV/vis (DCM): λ_{max} nm (log ε): 719 (5.17), 689 (5.11), 654 (4.64), 625 (4.51), 402 (4.59), 360 (4.46). MS (MALDI-TOF) *m/z*: calcd 1107.0; found 1107.7 [M − H]⁺.
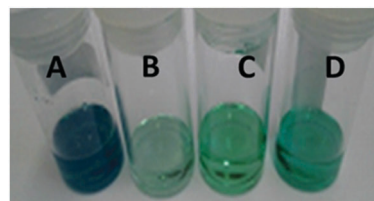

Fig. 3 Colour changes observed for the C_s (A), C_{4h} (B), D_{2h} (C) and C_{2v} (D) isomers in DCM.

Fraction C (D_{2h} symmetry isomer). IR [(KBr) ν_{max}/cm^{-1}]: 1247 (C–O–C); 1362 (CH$_3$); 1485, 1506, 1583 (C=C); 2865, 2957, (–C–H); 3036, 3288 (=C–H), UV/vis (DCM): λ_{max} nm (log ε): 718 (5.03), 688 (4.97), 658 (4.49), 626 (4.36), 353 (4.59), 334 (4.68). MS (MALDI-TOF) *m/z*: calcd 1107.0; found 1107.7 [M − H]⁺.

Fraction D (C_{2v} symmetry isomer). IR [(KBr) ν_{max}/cm^{-1}]: 1248 (C–O–C); 1362 (CH$_3$); 1477, 1506, 1589 (C=C); 2856, 2924, 2957 (–C–H); 3297 (=C–H), UV/vis (DCM): λ_{max} nm (log ε): 715 (5.04), 687 (5.00), 657 (4.75), 627 (4.56), 360 (4.88), 334 (4.99). MS (MALDI-TOF) *m/z*: calcd 1107.0; found 1107.7 [M − H]⁺.

2.4 Z-scan measurements

The experimental second order NLO parameter was determined by measuring the normalised transmittance from an open aperture Z-scan experiment. The normalised transmittance is given by eqn (1):[21,22]

$$T_n(z_s) = \frac{1}{Aq_0(Z_s)}\int_{-\infty}^{+\infty}\ln[1 + q_0(z_s)f(\tau)]d\tau \quad (1)$$

where $f(\tau)$ is a function of time describing the temporal profile of the pulse for Gaussian pulses and has the form $f(\tau) = e^{(-\tau^2)}$. A is a normalization constant equal to $\int_{-\infty}^{+\infty}f(\tau)d\tau$ and $q_0(z_s)$ is a parameter characterizing the strength of the nonlinearity. When a circular Gaussian beam is used, q_0 is represented by eqn (2):[19,20]

$$q_0(z_s) = \frac{2\beta P_0 L_{eff}}{\pi w^2(z_s)} \quad (2)$$

where β is the nonlinear absorption coefficient of the material, P_0 is the peak power of the pulses and the L_{eff} the effective propagation length in the material, given by the relation:

$$L_{eff} = \frac{1 - e^{-(\alpha L)}}{\alpha} \quad (3)$$

where L is the sample length (or the thickness of the sample respectively) and α is the linear absorption coefficient. α is determined using eqn (4):

$$\alpha = \frac{h\nu}{N}\beta \quad (4)$$

where N corresponds to the number of active species per unit volume, h is Planck's constant and ν the frequency of a laser excitation. The parameter $w(z_s)$ (in eqn (2)) is the beam width at the sample plane defined as the distance from the beam centre

This journal is © The Royal Society of Chemistry 2015

J. Mater. Chem. C, 2015, **3**, 10705–10714 | **10707**

to the point where the intensity reduces to $1/e^2$ of its axis value. $w(z_s)$ and is defined by eqn (5):[21]

$$w(z_s) = w_0 \sqrt{1 + \left(\frac{z_s - z_0}{z_R}\right)^2} \qquad (5)$$

where w_0 is the beam width at the focal point and z_0 is the location of the beam focus. The parameter z_R is the Rayleigh length, defined by eqn (6):

$$z_R = \frac{\pi w_0^2}{\lambda} \qquad (6)$$

where λ is the beam wavelength. Eqn (1)–(6) are used to determine the nonlinear absorption coefficient (β) from experimentally measured transmittance. Tsigaridas et al.[21] produced an analytical formula, which is provided as eqn (7):

$$q_0(z_s) = \begin{cases} a_0 + a_1 T_n(z_s) + a_2 T_n^2(z_s) + a_3 T_n^3(z_s) & \text{for } T_n(z_s) \leq 0.75 \\ c_0 + c_1 [T_n(z_s)]^{c_2} & \text{for } T_n(z_s) \geq 0.75 \end{cases} \qquad (7)$$

where the coefficients $a_0, a_1, a_2, a_3, c_0, c_1, c_2$ for Gaussian pulses are given as 15.66, -37.45, 30.76, -8.97, -2.301, 2.156, -1.563, respectively.[21] Eqn (7) provides the $q_0(z_s)$ values directly from the normalized transmittance $T_n(z_s)$. The authors demonstrated that their technique enables the straightforward determination of β and is very robust to the presence of signal noise.[21] The absorption coefficient (β), as well as the beam parameters z_0 and z_R can be determined from the $q_0(z_s)$ values obtained from eqn (7). Substituting eqn (5) into eqn (2), $q_0(z_s)$ is then defined by eqn (8):

$$q_0(z_s) = \frac{Q_0}{1 + (z_s - z_0)^2 / z_R^2} \qquad (8)$$

where:

$$Q_0 = \frac{2\beta P_0 L_{eff}}{\pi w_0^2} = \frac{2\beta P_0 L_{eff}}{\lambda z_R} \qquad (9)$$

Eqn (7) gives a Gaussian plot with Q_0 as the maximum value at the beam waist ($z_s = z_0$). The full width at half maximum (FWHM) of the $q_0(z_s)$ is equal to $2z_R$. The peak value and the FWHM of the plot provides the values for Q_0 and z_R. Eqn (10) is then used to calculate the nonlinear absorption coefficient (β).

$$\beta = \frac{\lambda z_R Q_0}{2 P_0 L_{eff}} \qquad (10)$$

The imaginary component of the third order optical susceptibility $Im[\chi^{(3)}]$ is directly proportional to β via eqn (11):[23]

$$Im[\chi^{(3)}] = \frac{(n^2 \varepsilon_0 c \lambda \beta)}{(2\pi)} \qquad (11)$$

in which c and n, respectively, are the speed of light in a vacuum and the linear refractive index of the system. ε_0 is the permittivity of free space and λ is the wavelength of the laser light. At a molecular level, there is a direct correlation of $Im[\chi^{(3)}]$ with the imaginary hyperpolarizability, $Im(\gamma)$, which provides the

nonlinear absorption per mole of the sample via the relationship shown by eqn (12):[24,25]

$$Im(\gamma) = \frac{Im[\chi^{(3)}]}{N^* f^4} \qquad (12)$$

where $N^* = C_{mol} N_A$ (with C_{mol} being the concentration in mol) and f represents Lorenz local field factor and is given by eqn (13):

$$f = \frac{n^2 + 2}{3} \qquad (13)$$

2.5 DFT calculations

The first static hyperpolarizability (β_{ijk}) of a $3 \times 3 \times 3$ matrix with 10 components was calculated by performing DFT calculations according to literature methods.[17] The magnitude of the effective hyperpolarizability was determined from β_{ijk} using eqn (14):[17]

$$\beta_{eff} = [(\beta_{xxx} + \beta_{xyy} + \beta_{xzz})^2 + (\beta_{yyy} + \beta_{yzz} + \beta_{yxx})^2 + (\beta_{zzz} + \beta_{zxx} + \beta_{zyy})^2]^{1/2} \qquad (14)$$

Since the β_{ijk} values that are provided by the Gaussian 03 software are reported in Debye, Å², the calculated β_{eff} values were converted to electrostatic units (esu), (1 Å² = 1 × 10⁻³⁰ esu).

3. Results and discussion

3.1 Characterisation of the positional isomers using nonlinear optical (NLO) parameters and DFT calculations

Strong nonlinear absorption behaviour, with reverse saturable absorption (RSA) profiles, was observed for all of the isomers studied, Fig. 4. The nonlinear absorption coefficient (β), third order optical susceptibility ($Im[\chi^{(3)}]$) and hyperpolarizability (γ) values were determined for all of the isomers, Tables 1 and 2. The β values were obtained by a nonlinear fit of $q_0(z_s)$, a parameter that characterises the strength of the nonlinearity in the curve depicted in Fig. 4, using eqn (8) and (10) above. The measured β values for the isomers display a trend in which (Fraction B) C_{4h} (34.0 × 10⁻⁵ m MW⁻¹) > (Fraction D) D_{2h} (28.8 × 10⁻⁵ m MW⁻¹) > (Fraction A) C_{2v} (22.8 × 10⁻⁵ m MW⁻¹) > (Fraction C) C_s (13.7 × 10⁻⁵ m MW⁻¹).

The measured β values lie within the range of those reported previously for phthalocyanine complexes.[9,26,27] In the absence of single crystals suitable for use in X-ray crystallography, the symmetry labelling for the four fractions was determined using DFT by analyzing the calculated β values, since β values are known to be very sensitive to symmetry.[11] Table 1 gives the measured and DFT calculated β values, which were used to identify the symmetry of the Pc in each fraction. The theoretical β values suggest that the C_{4h} isomer is the most active and is responsible for most of the observed overall NLO response when measurements are made with a mixture of isomers.

It is known that nonlinearity increases with asymmetry when absorption by the excited state predominates.[28] The observed
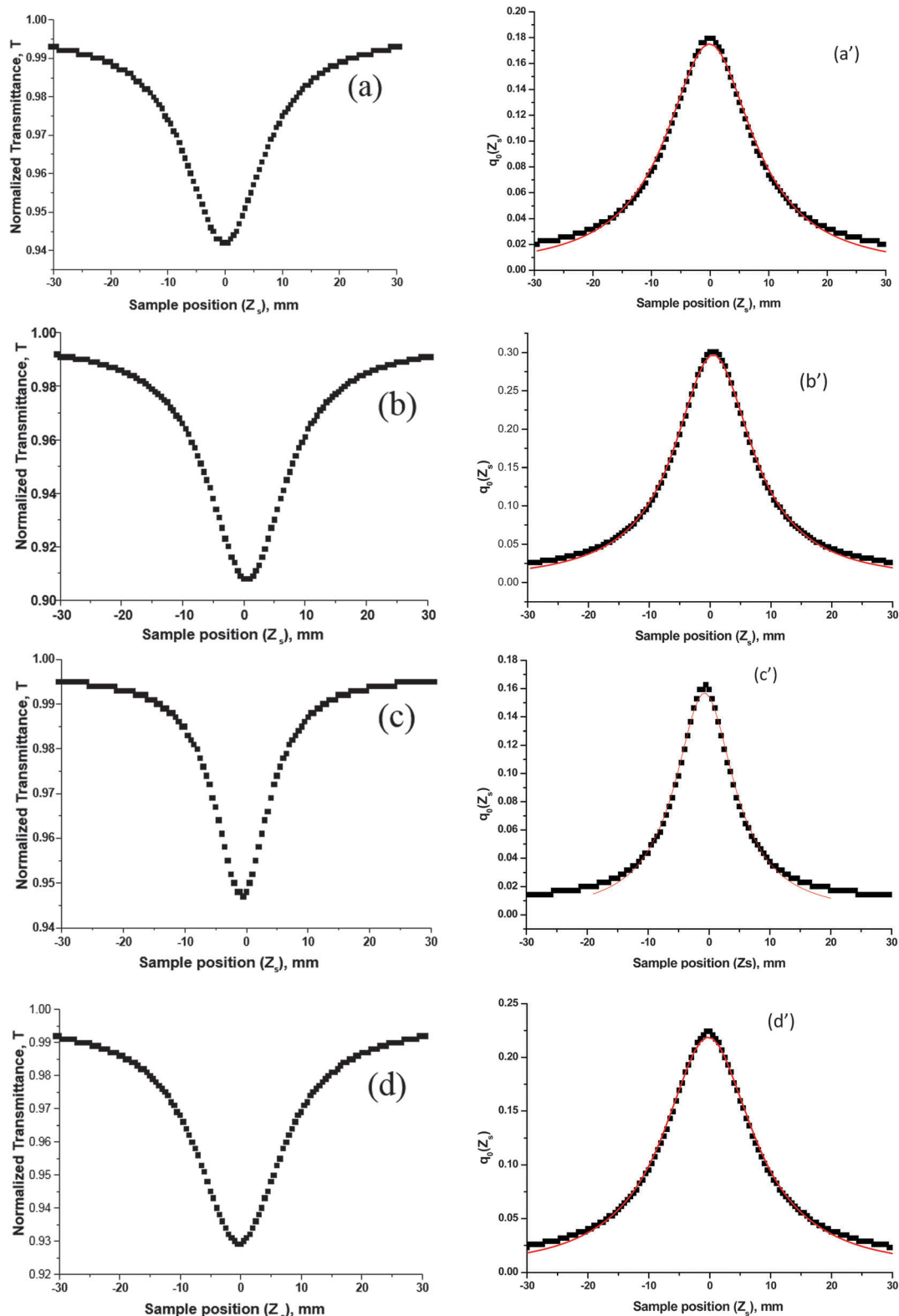
Fig. 4 Z-scan (a–d) and nonlinear fit (a′–d′) curves ($q_0(z_s)$) for (a) C_s-H_2Pc, (b) C_{4h}-H_2Pc, (c) D_{2h}-H_2Pc and (d) C_{2v}-H_2Pc. All experiments were conducted in DCM solution.

trends suggest that the C_{4h} isomer possesses the most efficient acentric order in terms of β values. The C_{2v} isomer shows a greater efficiency with respect to the C_s isomer. The C_s isomer has the least efficient acentric order. Efficient acentric molecular ordering is known to be the most important property for achieving a large bulk second order NLO response.

This journal is © The Royal Society of Chemistry 2015

J. Mater. Chem. C, 2015, **3**, 10705–10714 | **10709**

Table 1 Experimental and theoretical Z-scan results for second order nonlinear polarizability, β. DFT calculated with the B3LYP functional and 6-31G(d) basis sets

	Q_0	z_R (mm)	β (m MW^{-1}) $\times 10^{-5}$ (exp.)	β (theor.) (esu) $\times 10^{-28}$
C_{2v}	0.177	8.68	22.8	3.17
C_{4h}	0.297	7.74	34.0	4.61
C_s	0.157	5.91	13.7	2.49
D_{2h}	0.219	8.90	28.8	4.00

Table 2 Z-scan results for imaginary hyperpolarizability, Im(γ), and imaginary susceptibility, Im[$\chi^{(3)}$]

	Im[$\chi^{(3)}$] (esu)/α	Im(γ) (esu) $\times 10^{-31}$
C_{2v}	1.38×10^{-14}	1.11
C_{4h}	3.43×10^{-14}	2.32
C_s	2.30×10^{-14}	0.68
D_{2h}	2.91×10^{-14}	2.11

The optical susceptibility (Im[$\chi^{(3)}$]) and imaginary hyperpolarizability (Im(γ)) values are shown in Table 2. The optimal hyperpolarizability values for phthalocyanines in solution have been reported to lie within 10^{-34}–10^{-29} esu range.[24] The values determined for the series of isomers are all higher than the lower value in the range above. The measured Im(γ) values for the monomeric isomers follows a trend where C_{4h} (2.32 $\times$ 10^{-31} esu) > D_{2h} (2.11 $\times$ 10^{-31} esu) > C_{2v} (1.11 $\times$ 10^{-31} esu) > C_s (0.68 $\times$ 10^{-31} esu) respectively.

3.2 Characterisation of the positional isomers using solid state UV/visible and UV photoemission spectroscopy (UPS)

Fig. 5 contains the solid state electronic absorption spectra of D_{2h}, C_{4h}, C_{2v} and C_s isomers adsorbed on indium tin oxide (ITO) substrate. The spectra of the higher symmetry C_{4h} and D_{2h} isomers show the typical aggregation pattern for phthalocyanine compounds, whereby the aggregation peak is blue shifted with respect to the monomer peak. The blue-shifted peak is consistent with H aggregation of phthalocyanine molecules on the ITO substrate. The absorption spectra of the lower symmetry C_{2v} and C_s isomers exhibit a red-shifted aggregation peak with respect to the monomeric peak. This is consistent
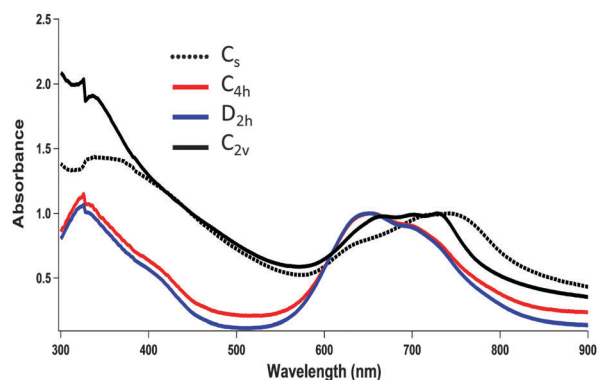
with J aggregation of phthalocyanine molecules on the ITO substrate. The stacking pattern is directed by the symmetry of the phthalocyanine molecules. The observed aggregation pattern helps to distinguish the fractions possessing the lower symmetry (C_{2v} and C_s) and higher symmetry (C_{4h} and D_{2h}) isomers. The different spectral properties of the two groups provides further support for the symmetry assignments that were made based on the β values obtained from the Z-scan technique. However the solid state absorption techniques are not sensitive enough to the relative orientations of the peripheral substituents to readily distinguish between the D_{2h} and C_{4h}, or C_s and C_{2v} isomers.

The UPS technique is sensitive enough to distinguish subtle differences between the four isomers in a solid state arrangement, Fig. 6. The secondary electron UPS spectra (Fig. 6a) determines the work function for each isomer while the valence band UPS spectra (Fig. 6b) shows the variance in HOMO onset from the Fermi level.

The work function and HOMO onset (E_F–HOMO) values from the UPS data are used to construct a schematic energy level diagram, Fig. 7, for the (A) C_s-H$_2$Pc, (B) C_{4h}-H$_2$Pc, (C) D_{2h}-H$_2$Pc and (D) C_{2v}-H$_2$Pc systems on bare ITO. The energy level diagram shows the different combinations of the work function and E_F–HOMO onset energies to determine the ionization potential (IP) energy level for each isomer. The differences in the work function and E_F–HOMO of the isomers could be due to variation in the thickness and pinning to the ITO. Hence the ionisation potential (IP) is the most important parameter to compare between the isomers. The work function and the E_F–HOMO values are added together to determine IP for each isomer. The low symmetry C_s and C_{2v} isomers are predicted to have similar ion IP of 5.02 and 5.04 eV, respectively, while the high symmetry D_{2h} and C_{4h} isomers are both predicted to have
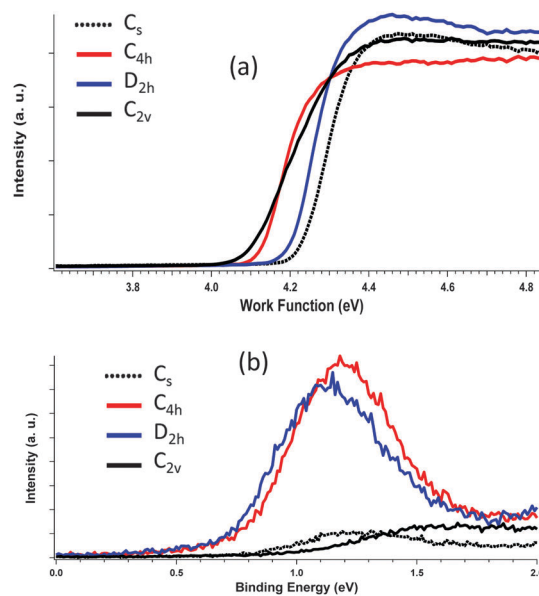

Fig. 5 UV-visible absorption spectra for C_{4h} (red line), D_{2h} (blue line), C_s (dotted line) and C_{2v} (black line) against an ITO background scan.

Fig. 6 (a) Onset of the secondary electron cut-off and (b) valence band UPS spectra for C_s-H$_2$Pc (dotted line), C_{4h}-H$_2$Pc (red line), D_{2h}-H$_2$Pc (blue line) and (4) C_{2v}-H$_2$Pc (black line) system on bare ITO.

Fig. 7 Schematic energy level diagram for the (A) C_s-H_2Pc, (B) C_{4h}-H_2Pc, (C) D_{2h}-H_2Pc and (D) C_{2v}-H_2Pc system on bare ITO.

values of 4.91 eV. UPS results matches with the solid state UV-visible absorption for the isomer symmetry pairing.

3.3 Electronic absorption and MCD spectroscopy

Electronic absorption spectroscopy is one of the most useful methods for characterizing phthalocyanines.[29] A D_{16h} symmetry $C_{16}H_{16}^{2-}$ cyclic polyene corresponding to the inner ligand perimeter with MOs arranged in an $M_L = 0, \pm1, \pm2, \pm3, \pm4, \pm5, \pm6, \pm7$ and 8 nodal property sequence can be regarded as being the parent hydrocarbon perimeter based on the magnetic quantum number for the cyclic perimeter, M_L. The four spin-allowed $M_L = \pm4 \rightarrow \pm5$ excitations give rise to two orbitally degenerate ^1E_u excited states, on the basis of the $\Delta M_L = \pm9$, and $\Delta M_L = \pm1$ transitions, resulting in the forbidden and allowed Q and B bands of Gouterman's 4-orbital model.[29] Michl[30–33] introduced an **a**, **s**, **−a** and **−s** terminology for the four MOs derived from the HOMO and LUMO of the parent perimeter so that π-systems of porphyrinoids with differing molecular symmetry can be readily compared, Fig. 8. Two of the MOs derived from the HOMO and the LUMO of the $C_{16}H_{16}^{2-}$ parent perimeter have nodal planes which coincide with the yz-plane and are referred to, respectively, as the **a** and **−a** MOs, while the corresponding MOs with antinodes are referred to as the **s** and **−s** MOs. Since the **a** and **s** MOs have angular nodal planes on alternating sets of atoms, Fig. 8, the incorporation of the aza-nitrogen atoms have a much larger stabilizing effect on the energy of the **s** MO resulting in a large separation of the **a** and **s** MOs and Q(0,0) bands that are dominated by the **a** $\rightarrow$ **−a** and **a** $\rightarrow$ **−s** one-electron transitions (Table 3).[34]

The electronic absorption spectra of the four positional isomers are almost identical, Fig. 9 and Table S1 as ESI,† as are the TD-DFT calculated spectrum that were carried out at the B3LYP/6-31G(d) level of theory for a series of positional isomers of an $H_2(OH)_4Pc$ model compound. Since no significant differences are observed or predicted in band energies that are related to the relative orientations of the peripheral substituents, optical spectral data cannot be used to definitively identify the four positional isomers. This is not surprising, since peripheral substituents are known have a relatively minor impact on the energies of the four frontier π-MOs, Fig. 8, in the absence of a large mesomeric interaction with the Pc π-system.[10]
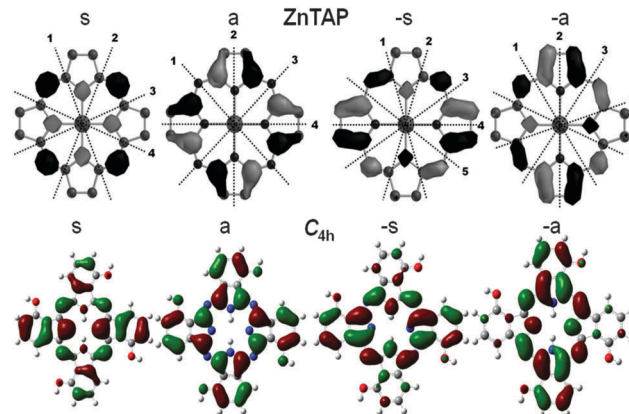

Fig. 8 Nodal patterns (top) of the four frontier π-MOs of zinc tetraaza-porphyrin (ZnTAP) with the angular nodal planes highlighted to describe the $M_L = \pm4$ and ±5 nodal patterns, and the nodal patterns of C_{4h} isomer of the $H_2(OH)_4Pc$ model compound at an isosurface value of 0.04 a.u. The MO energies (bottom) of the four positional isomers of the $H_2(OH)_4Pc$ model compound. The **a**, **s**, **−a** and **−s** MOs of Michl's perimeter model[30–33] are highlighted in gray. σ-MOs associated primarily with the aza-nitrogen lone pairs are offset to the right. Occupied MOs are denoted with small black diamonds. The HOMO–LUMO gap values are plotted against a secondary axis.

Table 3 Q band maxima in the absorption (Abs), and fluorescence excitation (Exc) and emission (Em) spectra, fluorescence lifetime (τ) and anisotropy rotational correlation time (Φ) values and molecular volumes (V_m) in DCM

| | λ_{max} (nm) | | | | | |
	Abs	Exc	Em	τ (ns)	Φ (ns)	V_m (10^{-27} m^3)
C_s	687:717	655	670	5.3 ± 0.02	0.360 ± 0.162	3.59
C_{4h}	686:717	652	682	5.3 ± 0.02	0.381 ± 0.198	3.80
D_{2h}	688:718	654	662	5.1 ± 0.02	0.339 ± 0.175	3.38
C_{2v}	689:716	653	665	5.0 ± 0.02	0.641 ± 0.376	6.39

MCD spectroscopy can be used to identify the main electronic Q(0,0) and B(0,0) bands, due to the presence of intense Faraday A_1 terms or coupled pairs of oppositely-signed Faraday B_0 terms.[10] The Stillman group[35–39] modified the band assignment on this basis to, in ascending energy, the Q (*ca.* 670 nm), B1 (*ca.* 370 nm), B2 (*ca.* 330 nm), N (*ca.* 275 nm), L (*ca.* 245 nm) and

This journal is © The Royal Society of Chemistry 2015

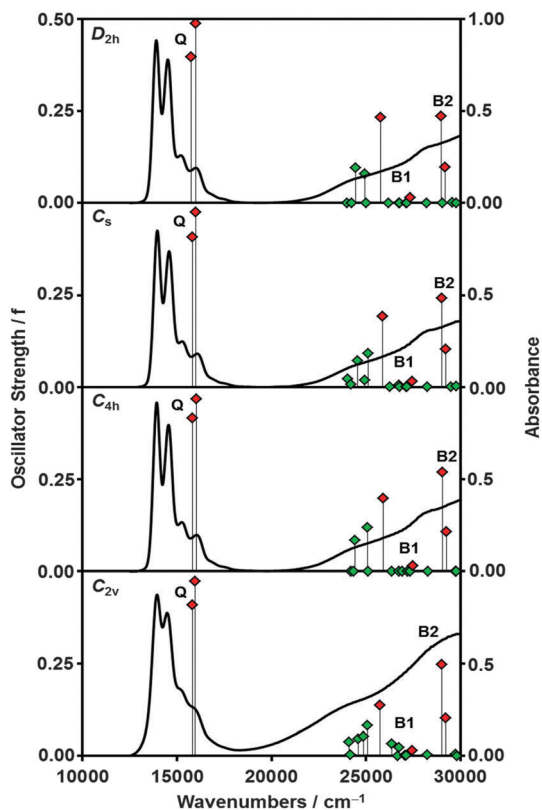*J. Mater. Chem. C*, 2015, **3**, 10705–10714 | **10711**

Fig. 9 Experimental and calculated spectra for the 4α-(4-*tert*-butyl-phenoxy)phthalocyanine positional isomers and the $H_2(OH)_4Pc$ model compounds, respectively. The experimental spectra were measured in DCM, while diamonds are used to denote the calculated bands. Red diamonds are used to highlight the Q, B1 and B2 bands.
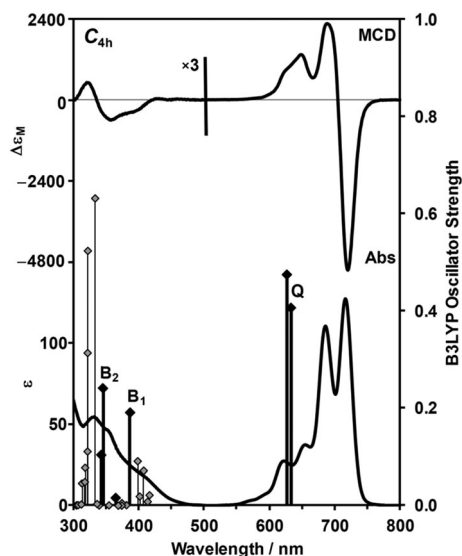

Fig. 10 UV-visible absorption and MCD spectra of the C_{4h} positional isomer of 4α-(4-*tert*-butylphenoxy) phthalocyanine. The spectra were measured in DCM. The calculated bands for the C_{4h} positional isomer of the $H_2(OH)_4Pc$ model compound are plotted against a secondary axis with darker black diamonds used to highlight the Q, B1 and B2 bands.

C (*ca.* 210 nm) bands.[36] Fig. 10 contains the absorption and MCD spectrum of the C_{4h} positional isomer. The presence of intense Faraday B_0 term intensity demonstrates that the B_1 and B_2 bands lie in the 300–400 nm region. The envelope of absorption intensity in the 400–470 nm region has been assigned previously to n → π* transitions associated with the lone pairs on the peripheral oxygen atoms,[40] or to the destabilizing effect of the electron donating effect of the sp³ hybridized oxygen atoms on the π-MOs that are associated primarily with the fused-ring-expansion of the ligand with benzo rings.[41] The presence of ππ* bands to the red of the B1 band in the TD-DFT calculations, Fig. 9, is broadly consistent with the latter explanation.

3.4 Fluorescence lifetimes and rotational correlation lifetimes

The excitation spectra of the D_{2h}, C_{4h} and C_s isomers were found to be identical to their ground state absorption spectra, but that of the C_{2v} isomer was not (see ESI†). The C_{2v} isomer may be more prone to aggregation than the other isomers. The fluorescence lifetimes for all four isomers lie in the 5.0–5.3 ns range, see Table 3, and fall within the range that is typically observed for monomeric phthalocyanine compounds.[42] The rotational correlation times for isomers C_s, C_{4h}, D_{2h} and C_{2v} were found to be 0.4, 0.4, 0.3 and 0.6 ns respectively. The C_{2v} isomer has a significantly greater correlation time than the other isomers. Differences in rotational correlation times are usually controlled by solvent viscosity, and the size and shape of the molecule.[14] The isomers were measured in the same solvent and have the same molecular weight, so any difference in rotational correlation times can be attributed to the differences in the molecular structures. The correlation times suggest that the C_{2v} isomer experiences a greater drag against the solvent molecules as it rotates compared to D_{2h}, C_{4h} and C_s isomers.

The rotational correlation times (ϕ) were used to calculate the molecular volume occupied by each isomer using eqn (15):[43]

$$\phi = \frac{\eta V}{kT} \qquad (15)$$

were k is the Boltzman constant, η the viscosity, V the molecular volume and T the absolute temperature. The results of molecular volume using the above equation are summarised in Table 1. The molecular volumes from eqn (15) are within range of theoretically calculated molecular volume of 1.29×10^{-27} m³ for an unsubstituted phthalocyanine compound. The unsubstituted phthalocyanine diameter was estimated to be13.5. The theoretical value was calculated from DFT optimised structures at the B3LYP/6-31G(d) level of theory. The D_{2h}, C_{4h} and C_s isomers are determined experimentally to have similar molecular volumes of 3.59×10^{-27}, 3.80×10^{-27} and 3.38×10^{-27} m³, respectively. The C_{2v} isomer has a molecular volume of 6.39×10^{-27} m³, which is approximately twice the measured molecular volume of isomer D_{2h}, C_{4h} and C_s. The four positional isomers are expected to have approximately the same molecular volume. The discrepancy observed for the C_{2v} isomer suggests that this isomer interacts with a greater number of solvent molecules and hence does not move as freely in DCM.

4. Conclusions

The four positional isomers of metal free 4α-(4-tert-butylphenoxy)-phthalocyanine have been successfully separated. The UV-visible absorption and MCD spectroscopy of the monomeric forms of the isomers have been studied. The fluorescence lifetimes of ~ 5 ns in DCM are similar in each case, and the D_{2h}, C_{4h} and C_s isomers have rotational times in the range of ~ 0.3 ns, while the C_{2v} isomer has a longer rotational time of ~ 0.6 ns. The viscosity values calculated on this basis, predict that the C_{2v} isomer has a greater viscosity value due to a greater interaction with the solvent molecules. Since TD-DFT calculations predict that the optical spectra of the four isomers are very similar, symmetry-sensitive Z-scan measurements were used to assign the different isomers by making using of the DFT calculated β values. These follow a similar trend to the experimentally derived γ values that were determined for each isomer. While the C_{4h} isomer displays an enhanced NLO response in terms of both the β and $Im(\gamma)$ values compared to the other isomers, smallest NLO response were observed for the C_{2v} and C_s isomers, respectively. Solid state UV-visible absorption spectroscopy and UPS data provide further support to the symmetry assignments.

Acknowledgements

References

1 G. de la Torre, P. Vázquez, F. Agulló-López and T. Torres, *J. Mater. Chem.*, 1998, **8**, 1671–1683.

2 T. Verbiest, S. Houbrechts, M. Kauranen, K. Clays and A. Persoons, *J. Mater. Chem.*, 1997, **7**, 2175–2189.

3 J. M. Fox, T. J. Katz, S. V. Elshocht, T. Verbiest, M. Kauranen, A. Persoons, T. Thongpanchang, T. Krauss and L. Brus, *J. Am. Chem. Soc.*, 1999, **121**, 3453–3459.

4 E. M. Maya, A. W. Snow, J. S. Shirk, R. G. S. Pong, S. R. Flom and G. L. Roberts, *J. Mater. Chem.*, 2003, **13**, 1603–1613.

5 M. A. Diaz-Garcia, *J. Porphyrins Phthalocyanines*, 2009, **13**, 652–667.

6 J. Britton, M. Durmus S. Khene, V. Chauke and T. Nyokong, *J. Porphyrins Phthalocyanines*, 2013, **17**, 691–702.

7 C. Mkhize, J. Britton and T. Nyokong, *Polyhedron*, 2014, **81**, 607–613.

8 J. Britton, M. Durmuş, V. Chauke and T. Nyokong, *J. Mol. Struct.*, 2013, **1054–1055**, 209–214.

9 C. Nitschke, S. M. O'Flaherty, M. Kroll, J. J. Doyle and W. J. Blau, *Chem. Phys. Lett.*, 2004, **383**, 555–560.

10 J. Mack and N. Kobayashi, *Chem. Rev.*, 2011, **111**, 281–371.

11 T. Verbiest, S. V. Elshocht, A. Persoons, C. Nuckolls, K. E. Phillips and T. J. Katz, *Langmuir*, 2001, **17**, 4685–4687.

12 Z. Li, Y. Liu, H. Kim, J. M. Hales, S. H. Jang, J. Luo, T. Baehr-Jones, M. Hochberg, S. R. Marder, J. W. Perry and A. K.-Y. Jen, *Adv. Mater.*, 2012, **24**, OP326–OP330.

13 S. D. Bella, *Chem. Soc. Rev.*, 2001, **30**, 355–366.

14 P. Tau and T. Nyokong, *Electrochim. Acta*, 2007, **52**, 3641–3650.

15 T. Nyokong and E. M. Antunes, *J. Porphyrins Phthalocyanines*, 2009, **13**, 153–160.

16 M. J. Frisch, G. W. Trucks, H. B. Schlegel, G. E. Scuseria, M. A. Robb, J. R. Cheeseman, J. A. Montgomery Jr., T. Vreven, K. N. Kudin, J. C. Burant, J. M. Millam, S. S. Iyengar, J. Tomasi, V. Barone, B. Mennucci, M. Cossi, G. Scalmani, N. Rega, G. A. Peters son, H. Nakatsuji, M. Hada, M. Ehara, K. Toyota, R. Fukuda, J. Hasegawa, M. Ishida, T. Nakajima, Y. Honda, O. Kitao, H. Nakai, M. Klene, X. Li, J. E. Knox, H. P. Hratchian, J. B. Cross, V. Bakken, C. Adamo, J. Jaramillo, R. Gomperts, R. E. Stratmann, O. Yazyev, A. J. Austin, R. Cammi, C. Pomelli, J. W. Ochterski, P. Y. Ayala, K. Morokuma, G. A. Voth, P. Salvador, J. J. Dannenberg, V. G. Zakrzewski, S. Dapprich, A. D. Daniels, M. C. Strain, O. Farkas, D. K. Malick, A. D. Rabuck, K. Raghavachari, J. B. Foresman, J. V. D. J. Fox, T. Keith, M. A. Al-Laham, C. Y. Peng, A. Nanayakkara, M. Challacombe, P. M. W. Gill, B. Johnson, W. Chen, M. W. Wong, C. Gonzalez and J. A. Pople, *Gaussian 03, Revision E.01*, Gaussian Inc., Wallingford, CT, 2004.

17 P. S. Liyanage, R. M. de Silva and K. M. N. de Silva, *THEOCHEM*, 2003, **639**, 195–201.

18 M. J. Frisch, G. W. Trucks, H. B. Schlegel, G. E. Scuseria, M. A. Robb, J. R. Cheeseman, G. Scalmani, V. Barone, B. Mennucci, G. A. Petersson, H. Nakatsuji, M. Caricato, X. Li, H. P. Hratchian, A. F. Izmaylov, J. Bloino, G. Zheng, J. L. Sonnenberg, M. Hada, M. Ehara, K. Toyota, R. Fukuda, J. Hasegawa, M. Ishida, T. Nakajima, Y. Honda, O. Kitao, H. Nakai, T. Vreven, J. A. Montgomery, Jr., J. E. Peralta, F. Ogliaro, M. Bearpark, J. J. Heyd, E. Brothers, K. N. Kudin, V. N. Staroverov, R. Kobayashi, J. Normand, K. Raghavachari, A. Rendell, J. C. Burant, S. S. Iyengar, J. Tomasi, M. Cossi, N. Rega, J. M. Millam, M. Klene, J. E. Knox, J. B. Cross, V. Bakken, C. Adamo, J. Jaramillo, R. Gomperts, R. E. Stratmann, O. Yazyev, A. J. Austin, R. Cammi, C. Pomelli, J. W. Ochterski, R. L. Martin, K. Morokuma, V. G. Zakrzewski, G. A. Voth, P. Salvador, J. J. Dannenberg, S. Dapprich, A. D. Daniels, Ö. Farkas, J. B. Foresman, J. V. Ortiz, J. Cioslowski and D. J. Fox, *Gaussian 09, Revision D.01*, Gaussian, Inc., Wallingford CT, 2009.

19 M. Kandaz, A. R. Özkaya and Ö. Bekaroğlu, *Monatsh. Chem.*, 2001, **132**, 1013–1022.

20 M. J. MacLachlan, in *Frontiers in Transition Metal-Containing Polymers*, ed. A. S. Abd-El-Aziz and I. Manners, Wiley & Sons, New York, 2007, pp. 208–216.

21 G. Tsigaridas, I. Polyzos, P. Persephonis and V. Giannetas, *Opt. Commun.*, 2006, **266**, 284–289.

22 M. Sheik-Bahae, A. A. Said, T. H. Wei, D. J. Hagan and E. W. Van Stryland, *IEEE J. Quantum Electron.*, 1990, **26**, 760–769.

23 E. M. García, S. M. O'Flaherty, E. M. Maya, G. de la Torre, W. Blau, P. Vázqueza and T. Torres, *J. Mater. Chem.*, 2003, **13**, 749–753.

24 D. Dini and M. Hanack, in *The Porphyrin Handbook: Physical Properties of Phthalocyanine-based Materials*, ed. K. M. Kadish, K. M. Smith and R. Guilard, Academic Press, USA, 2003, vol. 17, pp. 22–31.

25 J. Simon and C. Sirlin, *Pure Appl. Chem.*, 1989, **61**, 1625–1629.

26 P. T. Anusha, P. Silviya Reeta, L. Giribabu, S. P. Tewari and S. Venugopal Rao, *Mater. Lett.*, 2010, **64**, 1915–1917.

27 M. G. Kuzyk and C. W. Dirk, *Phys. Rev. A: At., Mol., Opt. Phys.*, 1990, **41**, 5098–5109.

28 J. Zhu, Y. Li, Y. Chen, J. Wang, B. Zhang, J. Zhang and W. J. Blau, *Carbon*, 2011, **49**, 1900–1905.

29 M. Gouterman, in *The Porphyrins*, ed. D. Dolphin, Academic Press, New York, 1978, vol. III, pp. 1–165.

30 J. Michl, *J. Am. Chem. Soc.*, 1978, **100**, 6801–6811.

31 J. Michl, *J. Am. Chem. Soc.*, 1978, **100**, 6812–6818.

32 J. Michl, *Pure Appl. Chem.*, 1980, **52**, 1549–1564.

33 J. Michl, *Tetrahedron*, 1984, **40**, 3845–3934.

34 J. Mack, Y. Asano, N. Kobayashi and M. J. Stillman, *J. Am. Chem. Soc.*, 2005, **127**, 17697–17711.

35 T. Nyokong, Z. Gasyna and M. J. Stillman, *Inorg. Chem.*, 1987, **26**, 548–553.

36 T. Nyokong, Z. Gasyna and M. J. Stillman, *Inorg. Chem.*, 1987, **26**, 1087–1095.

37 E. A. Ough, T. Nyokong, K. A. M. Creber and M. J. Stillman, *Inorg. Chem.*, 1988, **27**, 2724–2732.

38 J. Mack and M. J. Stillman, *J. Phys. Chem.*, 1995, **95**, 7935–7945.

39 J. Mack and M. J. Stillman, *Inorg. Chem.*, 1997, **36**, 413–425.

40 Z. Gasyna, N. Kobayashi and M. J. Stillman, *J. Chem. Soc., Dalton Trans.*, 1989, 2397–2405.

41 J. Mack, N. Kobayashi and M. J. Stillman, *J. Inorg. Biochem.*, 2010, **102**, 472–479.

42 N. Nombona, W. Chidawanyika and T. Nyokong, *J. Mol. Struct.*, 2012, **1012**, 31–36.

43 J. W. Borst, M. A. Hink, A. van Hoek and A. J. W. G. Visser, *J. Fluoresc.*, 2005, **15**, 153–160.